

Mechanical behavior and dynamic failure of high-strength ultrafine grained tungsten under uniaxial compression

Q. Wei ^{a,*}, T. Jiao ^b, K.T. Ramesh ^b, E. Ma ^b, L.J. Kecskes ^c, L. Magness ^c,
R. Dowding ^c, V.U. Kazykhanov ^d, R.Z. Valiev ^d

^a Department of Mechanical Engineering, University of North Carolina at Charlotte, 362, ERB, Charlotte, NC 28223, USA

^b Center for Advanced Metallic and Ceramic Systems, The Johns Hopkins University, MD 21218, USA

^c Army Research Laboratory, Aberdeen Proving Ground, MD 21005, USA

^d Ufa State Aviation Technical University, Ufa 450000, Russia

Received 21 June 2005; received in revised form 18 August 2005; accepted 19 August 2005

Available online 6 October 2005

Abstract

We have systematically investigated the quasi-static and dynamic mechanical behavior (especially dynamic failure) of ultra-fine grained (UFG) tungsten (W) under uniaxial compression. The starting material is of commercial purity and large grain size. We utilized severe plastic deformation to achieve the ultrafine microstructure characterized by grains and subgrains with sizes of ~ 500 nm, as identified by transmission electron microscopy. Results of quasi-static compression show that the UFG W behaves in an elastic–nearly perfect plastic manner (i.e., vanishing strain hardening), with its flow stress approaching 2 GPa, close to twice that of conventional coarse grain W. Post-mortem examinations of the quasi-statically loaded samples show no evidence of cracking, in sharp contrast to the behavior of conventional W (where axial cracking is usually observed). Under uniaxial dynamic compression (strain rate $\sim 10^3$ s⁻¹), the true stress–true strain curves of the UFG W exhibit significant flow softening, and the peak stress is ~ 3 GPa. Furthermore, the strain rate sensitivity of the UFG W is reduced to half the value of the conventional W. Both in situ high-speed photography and post-mortem examinations reveal shear localization and as a consequence, cracking of the UFG W under dynamic uniaxial compression. These observations are consistent with recent observations on other body-centered cubic metals with nanocrystalline or ultrafine microstructures. The experimental results are discussed using existing models for adiabatic shear localization in metals.

© 2005 Acta Materialia Inc. Published by Elsevier Ltd. All rights reserved.

Keywords: Tungsten; Ultrafine microstructure; Severe plastic deformation; Strain rate sensitivity; Flow softening

1. Introduction

Plastic instability may be manifested in the form of shear banding when the usual stabilizing mechanisms (such as strain hardening and strain rate hardening) are diminished, and the destabilizing mechanisms (such as thermal or geometric softening) prevail [1–5]. In many applications this plastic localization is to be avoided; yet in some others it is a desirable deformation mode. In particular, the use of

tungsten (W) or tungsten heavy alloys (WHA) to make high-density kinetic energy anti-armor penetrators requires that the materials exhibit “self-sharpening” behavior, at least under high loading (strain) rates [6–8]. For this to happen plastic flow needs to be localized such that cracks form at desirable strain levels only in these heavily deformed shear bands to discard pieces of the material along the penetration path. However, W is known to be notoriously resistant to adiabatic shear banding. One reason for this is the high ductile-to-brittle transition temperature (DBTT) of W [9,10], which causes cracking at many locations in the material prior to the accumulation of the plastic dissipation needed to trigger plastic instabilities.

* Corresponding author. Tel.: +1 704 687 8213; fax: +1 704 687 8345.
E-mail address: qwei@uncc.edu (Q. Wei).

Recently, both non-adiabatic and adiabatic shear banding have been reported in some body-centered cubic (bcc) metals with ultrafine grain (UFG) or nanocrystalline (NC) microstructures [11–17]. The UFG or NC microstructures can be achieved through different technologies, including powder metallurgy [11,13–15] and severe plastic deformation (SPD) [12,16]. It is worth noting that most such investigations have been based on existing theoretical frameworks for shear bands in metals [12]. We have also reported some preliminary observations of plastic shear localization in bulk W with ultrafine microstructure [18]. In the present paper, we present a systematic in-depth investigation of the processing, microstructure and the quasi-static and dynamic mechanical behavior, especially the dynamic failure of high-strength UFG W under uniaxial compression. To avoid contamination from impurities which have been held responsible for the embrittlement of powder-metallurgy-processed W, we used SPD to refine the microstructure of conventional W with commercial impurity levels. The microstructure was analyzed using transmission electron microscopy (TEM). The UFG W has been tested at both quasi-static loading rates ($10^{-4} - 10^0 \text{ s}^{-1}$) and dynamic loading rates ($\sim 10^3 \text{ s}^{-1}$, using a compression Kolsky bar). We used a high-speed camera that is able to capture eight frames at a maximum rate of 10^8 fps (frames per second) to record the dynamic deformation and failure process. The plastic deformation and failure mechanisms were also investigated by observing the surfaces of the post-mortem samples using optical microscopy and scanning electron microscopy (SEM).

2. Experimental details

Based on observations on other bcc metals such as Fe [11,12,14,15,17], V [13] and Ta [16], we started with a commercial purity W with large grain size ($\sim 40 \mu\text{m}$), and used equal channel angular pressing (ECAP) [19–24] to refine the grain size or microstructure. At temperatures above $1250 \text{ }^\circ\text{C}$, recrystallization takes place rapidly in deformed W [25,26]. The recrystallization temperature is a function of impurity level and the amount of plastic deformation [9]. In this work, to ensure the efficiency of grain refinement during ECAP, the processing temperature was around $1000 \text{ }^\circ\text{C}$. The work piece was encapsulated in a stainless steel canister to reduce oxidation. Due to the relatively poor workability of coarse-grained (CG) W, the die angle for ECAE is 120° to avoid cracking during ECAP. Compared to a right angle die, the effective strain introduced through each individual pass is reduced [21], but this can be compensated for by increasing the number of passes. Fig. 1(a) displays an optical micrograph of a W sample that went through four passes of ECAP of route B_c [21]. Microstructure refining is apparent (from the original $\sim 40 \mu\text{m}$ to a few μm).

To further refine the microstructure down into the ultrafine regime, a piece of the ECAP W was machined off and rolled in a confined manner at successively lowered temper-

atures starting at $800 \text{ }^\circ\text{C}$, with the final rolling temperature being $600\text{--}700 \text{ }^\circ\text{C}$. The rolling plane was perpendicular to the extrusion direction of the ECAP die. The additional equivalent von Mises strain introduced through this low temperature rolling was about 1.8. The TEM micrographs of Fig. 1(b) and (c) suggest that the grain size and sub-grain size have been refined to $\sim 500 \text{ nm}$. Selected area diffraction patterns (not shown) indicate the presence of both large angle and small angle grain boundaries.

Samples for quasi-static and dynamic mechanical testing were machined from the SPD processed W. An MTS servohydraulic loading system was used to measure the quasi-static behavior under uniaxial compression (sample dimensions meeting ASTM standards; strain rates 10^{-4} – 10^0 s^{-1}). Loading was along the channel direction for the ECAP samples, and normal to the rolling plane for the further rolled samples. For dynamic loading, we used the uniaxial compression Kolsky bar technique [27] where the specimen is sandwiched between two elastic bars (called the input and output bars). Strain gages are cemented on the elastic bars to measure (i) the incident pulse generated by an impacting projectile, (ii) the reflected pulse from the input bar/specimen interface and (iii) the pulse transmitted through the specimen to the output bar. Details of the Kolsky bar technique can be found in [27]. The interfaces between the specimen and the bars were carefully lubricated to minimize friction. The side faces of the specimens were polished to a mirror finish in order to observe the plastic deformation processes of the specimens under both quasi-static and dynamic compressive loadings. In the dynamic loading case, a DRS Hadland Ultra 8 high-speed camera with the ability to record eight frames at 10^8 frames per second was synchronized with the Kolsky bar system to record the dynamic deformation of the specimens. A schematic of the dynamic experimental setup is provided in Fig. 2. The purpose of using high-speed photography was to clarify whether and when shear bands are developed, their evolution during the plastic deformation of the material, and the dynamic failure of the specimens. For comparison, quasi-static and dynamic compressive tests were also performed on control samples, i.e., CG W. Post-mortem examinations of the samples were conducted using either optical microscopy or SEM. For some post-loading samples, the roughened side faces were polished away, and this was followed by chemical etching using the standard Murakami solution to reveal the microstructures of the shear bands.

3. Experimental results

There have been a number of papers in the literature dealing with the mechanical properties of powder metallurgy, conventional CG W under both quasi-static and dynamic loading conditions [28,29]. The results obtained in this work for the control CG W samples are consistent with what has been reported and are not presented here. Briefly, at room temperature and under quasi-static compression

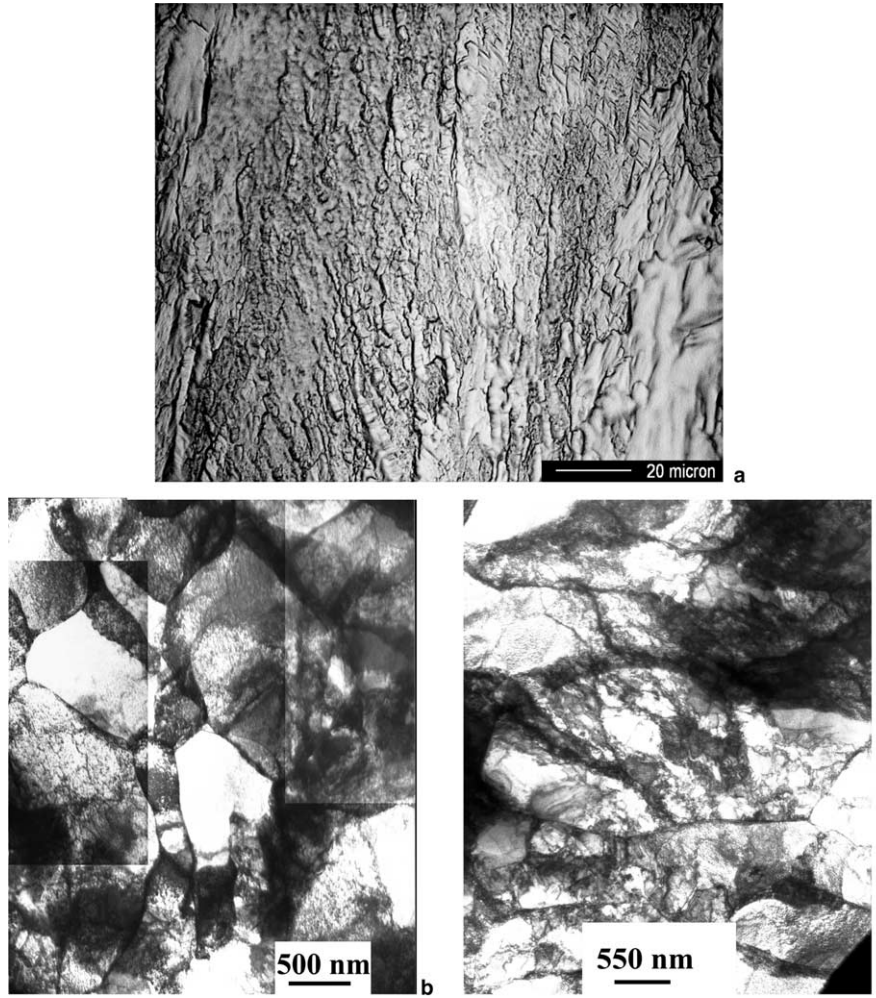


Fig. 1. Optical micrograph (a) of a W sample after four passes of ECAE at 1000 °C. Compared to the original coarse grain (~40 μm) microstructure (not shown here), the refinement of the microstructure is apparent. Transmission electron micrographs of SPD-processed (ECAP + rolling) UFG W (b, c), showing grains and dislocation cell structures refined to sizes of the order of 500 nm. Selected area diffraction (not shown here) shows the presence of both large angle and small angle grain boundaries.

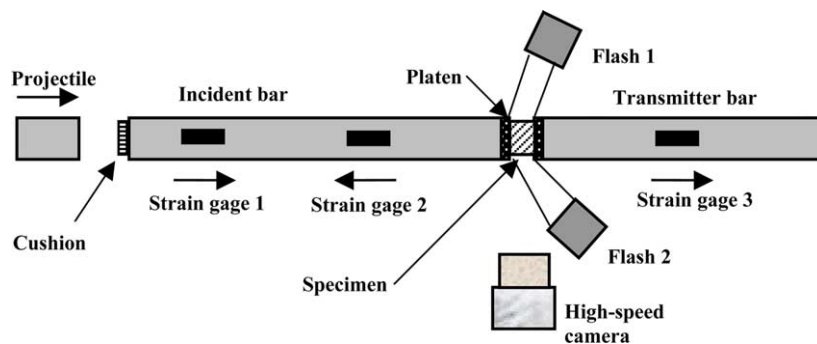


Fig. 2. Schematic of experimental setup for Kolsky bar compressive test with a high-speed camera synchronized with the system. Strain gages 1, 2, 3 are used for the high-speed camera, the incident/reflected and transmitted waves, respectively. The platens are a set of impedance-matched tungsten carbide disks collared with Ti-6Al-4V for the protection of the bars.

CG W usually has a yield stress of ~1000 MPa. Under tension, commercial purity CG W breaks in a completely brittle manner at a stress level less than 500 MPa, mostly in an inter-granular fracture mode [9,25]. Under dynamic com-

pression, the yield stress is around 1200 MPa, with the value depending on the strain rate [28,29]. Apparent strain hardening is observed for CG W under both quasi-static loading and dynamic loading (compressive). Post-mortem

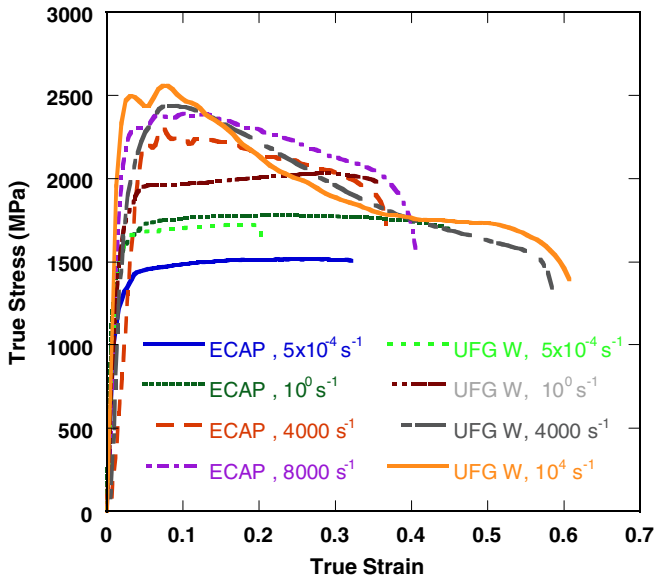


Fig. 3. True stress–strain curves of the ECAP W and the ECAP + CR (UFG) W, under uni-axial quasi-static, and dynamic (Kolsky bar) compressive loading. All the samples are rectangular with square loading faces. The quasi-static tests used strain rates $\sim 10^{-4}$ – 10^0 s^{-1} (MTS hydro-servo system). For the dynamic testing, the strain rate was determined by the projectile mass and the pressure, as well as the prescribed strain level.

examinations of the samples usually reveal axial cracks along the loading direction [28].

Fig. 3 displays the stress–strain curves under various strain rates (from quasi-static to dynamic) for the ECAP W and the W that was processed by ECAP at 1000 °C followed by cold-rolling (referred to hereafter as ECAP + CR W). ECAP at 1000 °C (six passes in this case) has elevated the quasi-static flow stress to ~ 1.5 times that of the CG W. ECAP has also markedly reduced the strain hardening. Cold rolling further strengthens the material until the flow stress is nearly doubled relative to the CG W. Under dynamic loading, both the ECAP W and the ECAP + CR W exhibit flow softening after small plastic strains, in contrast to the dynamic behavior of CG W where slight work hardening is observed. This flow softening is in part due to the accumulation of plastic work that is converted into heat during dynamic loading. Due to adiabatic heating, the sample's temperature may rise by

$$\Delta T = \frac{\beta}{\rho C_p} \int_0^{\varepsilon_f} \sigma d\varepsilon, \quad (1)$$

where β is the Taylor–Quinney coefficient which characterizes the fraction of plastic work converted into heat (assumed to be 0.9 in this case [5]), ρ is the density (19.25 g/cm³ for W), C_p is the specific heat (0.134 J/g K), σ is the flow stress and ε_f is the final strain for calculation. Assuming the isothermal stress–strain curve of the ECAP W and ECAP + CR W to be elastic–perfect plastic, Eq. (1) can be simply written as

$$\Delta T = \frac{\beta}{\rho C_p} \sigma \cdot \varepsilon_f. \quad (2)$$

For example, for a plastic strain of ~ 0.2 , the temperature rise in an ECAP W under dynamic loading would be around 140 °C using a flow stress of ~ 2.0 GPa, while for the ECAP + CR W, it would be around 210 °C using a flow stress of ~ 3.0 GPa. If the measured “plastic” strain has contributions from both local cracking and dislocation-mediated plastic deformation, an over-estimate will result from Eq. (1). This may be the case for the ECAP W. Fig. 4(a) shows a post-loading optical image of one side face of an ECAP W sample. Cracks nearly parallel to the loading axis are observed. Fig. 4(b) is an SEM micrograph showing the cracks more clearly. In both micrographs, loading is vertical. Thus, the micro-cracks are roughly parallel to the loading axis. This behavior is similar to that observed in an extruded W that exhibits a flow stress level close to the ECAP W in this work [28]. We presume that due to cracking, the actual adiabatic temperature rise would be less than the estimate from Eq. (2).

Though the peak flow stresses of the ECAP + CR W are higher than those of the ECAP W samples at the same strain rate, the flow softening is much more significant beyond a certain strain level. For example, the flow stresses of the ECAP + CR W are even lower than those of the ECAP W after about a true strain of 0.2. After that point, the stress–strain curves have a more negative slope for ECAP + CR W than for ECAP W. The following observations may provide an explanation.

Fig. 5(a) is an optical image of the side face of a dynamically tested ECAP + CR W sample. The loading is again vertical. Instead of cracks, obvious shear bands (SBs) are present. High-speed photography (shown later) indicates that the stress collapse corresponds approximately to the initiation and subsequent rapid growth of these shear bands. Fig. 5(b) displays an SEM micrograph, indicating that shear bands have been developed on two conjugated surfaces (the bright contrast in the micrograph indicated by arrows corresponds to SBs). Fig. 5(c) is an enlarged image of two shear bands corresponding to the left branch of Fig. 5(a). Shear localization is evident, with the band oriented at an angle of $\sim 40^\circ$ with respect to the loading direction. At high magnifications, such as Fig. 5(d–g), details of the microstructure in the shear band can be observed, including the very large localized shear flow during dynamic loading. In Fig. 5(g) and later in Fig. 6, one can see a crack as the result of the localized adiabatic shearing.

To further investigate the microstructure in the SB, the roughened surface was polished away, and then etched using a standard Murakami solution. Fig. 6 shows an optical image of the polished and etched surface (the loading axis remains vertical). Extensive plastic shear has been developed, presumably leading to subsequent cracking (also shown in Fig. 5(g)). A simple estimate can be obtained for the maximum shear strain experienced at the center of the adiabatic shear band (ASB) using the slope of the flow lines. As such, a shear strain of the order of ~ 3.0 can be estimated based on the information in Fig. 6. One can now use Eqs. (1) or (2) to estimate the adi-

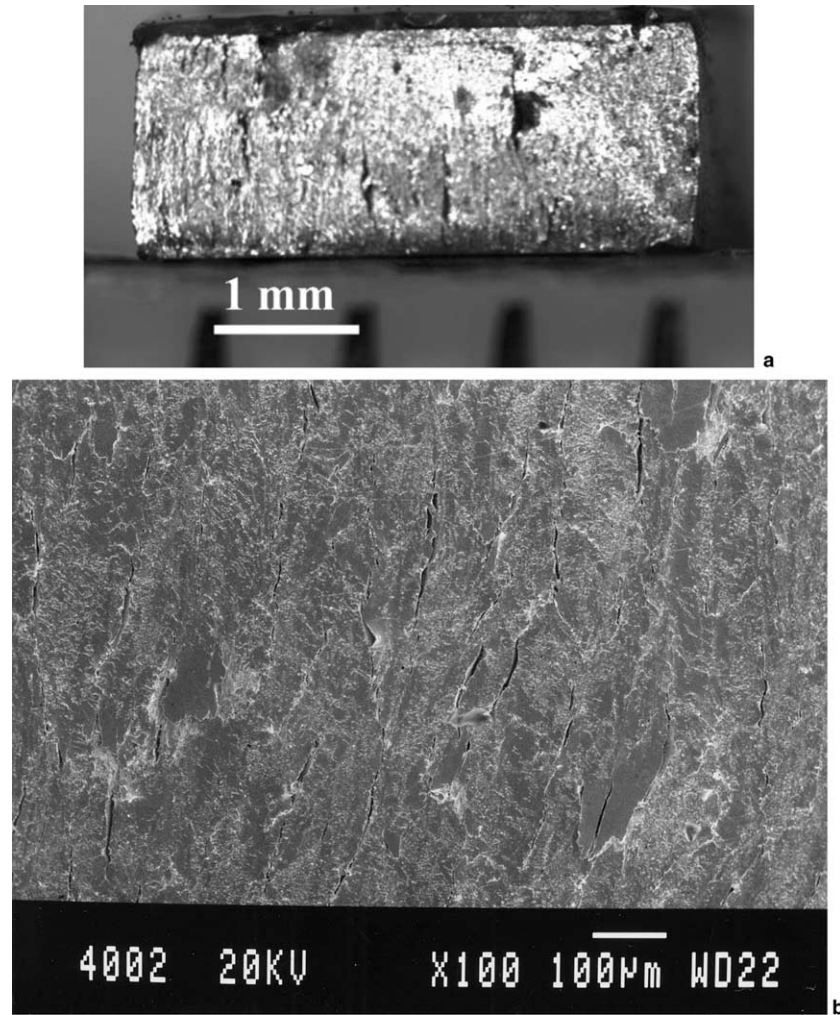


Fig. 4. (a) Post-mortem optical micrograph of dynamically loaded ECAP W (loading is vertical), showing cracks along the loading axes. (b) SEM micrograph of the same sample as (a) showing microcracks approximately parallel to the loading axis (vertical).

adiabatic temperature rise at the center of the band during dynamic loading, with a result of about 1400 K. Temperature rises as large as 1000 °C have been frequently reported for such loading conditions [5]. These shear bands do not show a well-defined central region that etches differently, unlike the shear bands observed in SPD Fe [12]. This suggests that the temperature rise might not be sufficient to incur extensive recrystallization in the center of the SB. TEM analysis of the shear band is under way to clarify the detailed processes involved. The flow lines suggest the canonical structure predicted for ASB [4], where the flow lines bend down through the boundary into the band, and then curve away on the other side forming an anti-symmetric pattern.

If the width of the region of concentrated flow lines is taken as the shear band width, Fig. 6 provides a width of $\sim 40 \mu\text{m}$. One way to show whether the shear bands are adiabatic is to compare the thermal conduction length scale over the time of the dynamic loading with the width of the shear band. A simple but close estimate of the thermal conduction length scale is $\sqrt{2\alpha \cdot \Delta t}$, where α is the thermal diffusivity of W ($0.662 \text{ cm}^2/\text{s}$ at room temperature and

$0.226 \text{ cm}^2/\text{s}$ at melting point [9]), and Δt is the time elapsed during dynamic loading (typically $\sim 100 \mu\text{s}$). Such an estimate results in a thermal conduction length scale in the order of $\sim 1.0 \mu\text{m}$, much smaller than the apparent shear band width ($\sim 40 \mu\text{m}$). This suggests that the shear bands observed in this work are indeed of adiabatic nature.

To investigate the dynamics of the shear banding process and its relation with other phenomena, a high-speed camera was synchronized with the Kolsky bar system. In situ high-speed photography shows the evolution of ASB and subsequent cracking of the specimen. Fig. 7 displays seven frames from one such experiment, together with the corresponding stress–time and stress–strain curves. The square symbols on the curves indicate the time or the strain at which each frame was taken (Fig. 7(a) and (b)). As in Fig. 3, very high flow stresses and significant flow softening are observed. The first frame was taken before plastic deformation occurred (Fig. 7(c)). The specimen is observed in reflected light from the flashes, and is the rhomboid outlined in Fig. 7(c). (The rhomboid is the projection of the specimen given the camera angle). The bright areas to the

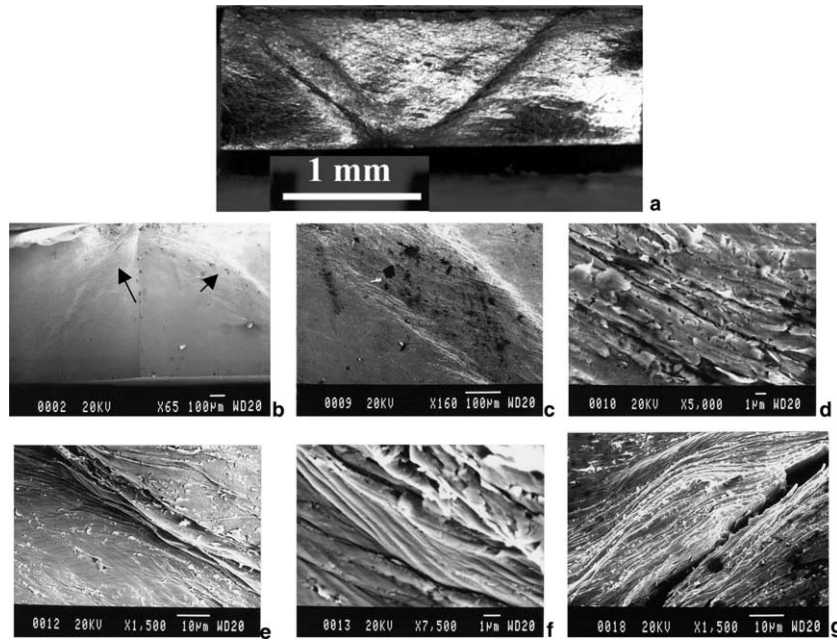


Fig. 5. (a) Post-mortem optical micrograph of adiabatic shear bands in dynamically loaded ECAP + CR W. (b) SEM micrograph showing adiabatic shear band on two conjugated side faces of an ECAP + CR W sample after dynamic loading. (c) is an enlarged SEM image of two shear bands corresponding to the left branch of (a). Shear localization is evident. (d) shows the details of the microstructure in the shear band. Notice the voids along with large, localized plastic deformation. (e) and (f) are microstructures as a result from the very large localized shear flow during dynamic loading. In (g), one can see a crack as the result of the localized adiabatic shearing.

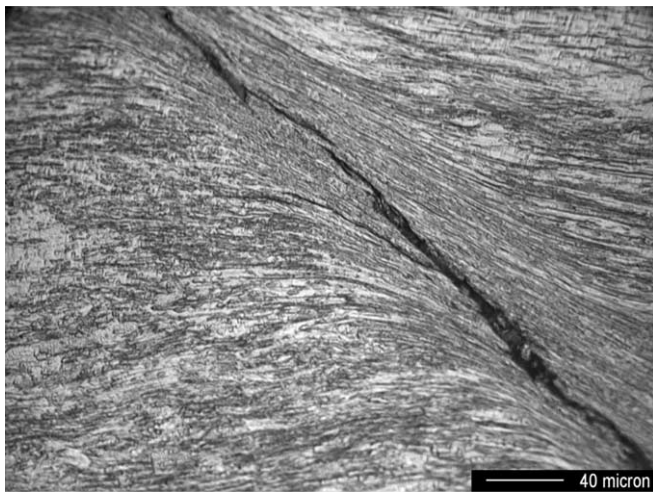


Fig. 6. Morphology of ASB and crack as revealed by chemical etching. Flow lines are clearly observed.

left and right of the specimen are reflections of the specimen in the polished ends of the bars. Compression occurs along the horizontal axis, with the incident wave arriving at the specimen/input-bar interface from the left. Fig. 7(d) is a frame captured about 20 μ s after (c), (at a strain of ~ 0.1). The upper left corner shows some dark contrast that indicates the initiation of shear localization. The time difference between subsequent consecutive frames is 4 μ s. In Fig. 7(e) (at a strain of about 0.15), the shear band formation is obvious as is the overall compression of the sample. Fig. 7(f) shows the initiation of a second

shear band from the upper right corner. Later frames (Fig. 7(g)–(i)) show the evolution of the shear bands, and by Fig. 7(i) well-defined ASBs can be identified.

In summary, our experimental results show that, compared to the unprocessed coarse-grain microstructure, SPD processed UFG W sustains much higher flow stresses under both quasi-static and dynamic loading. Compared to the CG W, the quasi-static true stress–true strain curves of SPD W behave in an elastic–nearly perfect plastic manner, i.e., with vanishing strain hardening. Under uniaxial dynamic compressive loading, significant flow softening is observed in the UFG W. Both post-mortem microscopic observations and in situ high-speed photography reveal intensive plastic shear localization in the UFG W, and the latter indicates that the shear localization takes place at a very small strain level. Cracking has also been observed as a consequence of the severe adiabatic shear localization in the UFG W.

4. Discussion

At this point, it is worth pointing out that even at liquid nitrogen temperature (77 K or -196 °C) and under tension single crystal W can be deformed plastically to large plastic strains at various orientations [30]. This is consistent with the behavior of other metals with bcc structure. However, conventional polycrystalline CG W behaves more like a brittle ceramic, especially under tension. This brittleness has largely been attributed to the weakening effect of the soluble interstitial impurities segregated along the grain

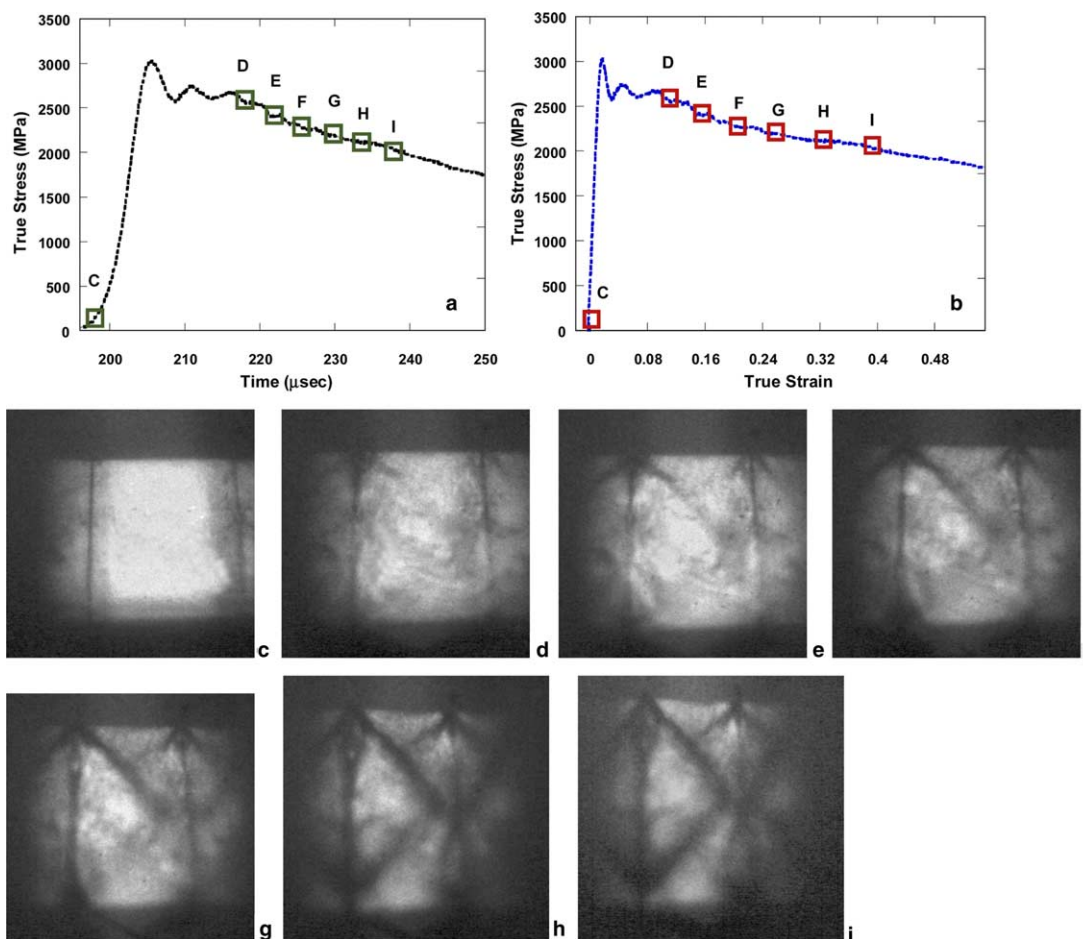


Fig. 7. The stress–time curve (a) and stress–strain curve (b) for a uniaxial compression Kolsky bar test of an SPD UFG W. The square boxes in each figure indicate the time or strain level at which each frame was captured. The letters above the square boxes in (a) and (b) correspond to the frames (c–i). From (c) to (i), seven frames are shown corresponding to the first seven time or strain points in (a, b). The loading wave came from the left horizontally. The final rolling temperature for this sample is 700 °C.

boundaries [9]. Therefore, the DBTT of CG W is dependent on the purity level of the material, the population density of grain boundaries, etc. [9]. CG W of commercial purity usually exhibits a DBTT above 150 °C [25,26,31]. This explains the ceramic-like behavior of such W at room temperature. Under dynamic loading, cracking usually preempts dislocation-mediated plastic deformation, and thus disallows accumulation of plastic work and the subsequent heating that is needed to trigger adiabatic shear localization.

One strategy to reinstate the ductility of W would be by refining the grain size of a CG W effectively so that the impurities can be re-distributed along the new grain boundaries. We did not favor the traditional powder metallurgy technology for the processing of UFG or nanostructured W since that may introduce more impurities, even though industrial consolidation of W powder is usually performed in a hydrogen atmosphere [9]. Conventional rolling or extrusion might be useful to refine the microstructure, but the reduction in the size of the work piece with each pass of processing greatly limits the final size of the work piece, and hence the maximum amount of plastic deforma-

tion that can be pumped into the work piece. An additional disadvantage associated with conventional rolling or extrusion is the limit in the misorientation of dislocation cells (the so-called incidental dislocation boundaries or IDBs, (see, e.g. [32–34]). For such boundaries, approximately 3° has been reported to be the saturated misorientation for von Mises strains above 4.5 [32,34], and therefore a limit for the final effective grain size. It is also to be noted that small angle grain boundaries such as achieved through rolling are usually of low energy, hence not as efficient as large angle grain boundaries at hosting interstitial impurities and thus decreasing the average impurity atom concentrations along the grain boundaries. Added to these disadvantages is the texture developed during large strain rolling or extrusion [33]. Since ECAP has been proven to be efficient to refine the grain size of most metals with relatively large angle grain boundaries (the angle distribution depends on the route and number of passes, for details, see [21]), we have adopted this technique for the refinement of grain size. Our experimental results in Fig. 3 for the ECAP W do indicate that ECAP helps elevate the strength level significantly. It has been asserted that grain boundaries in

metals processed by severe plastic deformation such as ECAP or high-pressure torsion are usually of high angle ($>15\text{--}20^\circ$) and non-equilibrium nature (with a grain boundary energy much higher than that of the equilibrium ones) [21,35–38]. Valiev et al. [35,36] further proposed that the SPD induced non-equilibrium and large angle grain boundaries explain the paradox of strength and ductility in metals so processed. We envisage, for W in particular, that the SPD induced non-equilibrium and large angle grain boundaries play important roles in diluting away the malignant impurities along the pre-existing grain boundaries by diffusion to and re-distribution along the newly created grain boundaries. The flow softening of even the plain ECAP W indicates that at least part of the apparent strain is due to dislocation-mediated plastic deformation, unlike the CG W where only axial cracking is observed [28]. The ECAP process has driven the microstructure of a CG W into a few micrometer regime (Fig. 1(a)), instead of UFG regime. This is mainly because of the relatively high ECAP temperature (1000°C and above) and die geometry used in this work. Further work may be needed to lower the ECAP temperature if the grain size is to be refined to a greater degree. This work demonstrates that additional low temperature rolling can at least be supplementary to the relatively high temperature ECAP. It has been reported that cold rolling also produces certain amount of large angle grain boundaries (the so-called geometrically necessary boundaries, GNBs [34]).

A more in depth analysis is needed to determine the effect of refined grain size on the tendency for a bcc metal, such as W, to ASB. Qualitatively, there are a number of variables that affect the initiation and development of ASB [5]. They include: thermomechanical properties, microstructure of the material, the stress state and external loading conditions. The thermomechanical properties include density, specific heat, thermal conductivity (thermal diffusivity), strain hardening rate, thermal softening rate, and strain rate sensitivity. The factors from the microstructure include size, shape, spacing, orientation, population and distribution of second phase particles, inclusions and precipitates, as well as texture, porosity, imperfections and thermal stability of the microstructures. External conditions may include perturbations imposed externally, their amplitude, sharpness and distributions. Under quasi-static tension, non-adiabatic plastic instability can be predicted using the well-known Considère criterion for the rate-independent case and the Hart criterion for the rate-dependent case [39]. In both cases, one of the most critical parameters is the strain-hardening rate defined by $(\partial\sigma/\partial\varepsilon)$, where σ is the flow stress and ε the plastic strain.

Most closed-form analyses on ASB are based on a pure-shearing loading condition [1–5]. Under compression, several flow localization parameters can be used to qualitatively describe the propensity of a metal for flow localization [40]. Generally speaking, such parameters are functions of the flow stress and its thermal sensitivity, strain hardening behavior and the strain rate sensitivity

(SRS) of the material. Materials with high flow stresses (or high dissipation numbers following an energy consideration [41]), high thermal sensitivity, small strain hardening and small SRS are more susceptible to adiabatic flow localization under dynamic compression [18]. Usually, SRS, or m , is defined as the exponent in a power law fit: $\sigma/\sigma_0 = (\dot{\varepsilon}/\dot{\varepsilon}_0)^m$.

Our mechanical testing shows that the UFG W behaves in an elastic–nearly perfect plastic manner under quasi-static loading, as seen from the almost flat stress–strain curves after yielding (Fig. 3). This indicates that the high-density of defects and much refined microstructure produced during SPD has greatly reduced the strain hardening capability of the commercial polycrystalline W. It has been asserted in some face-centered cubic (fcc) metals such as Cu and Ni [42,43] that smaller grain size leads to decreased work hardening rate during plastic deformation. A recent analysis suggests that below a certain length scale (e.g., grain size), there is an intrinsic size effect on work hardening in metals [44]. The critical length scale is around $3\ \mu\text{m}$ for most metals. Below this, work hardening (through storage of dislocations, for example) scales inversely with the grain size. This size effect may also be understood on the basis of reduced slip length (or dislocation mean free path) with reduced grain size or cell size. The slip length becomes a constant more easily and rapidly in a fine-grained metal [42].

We evaluate the SRS parameter m using flow stress data recorded at a number of strain rates (in this work, at a fixed strain of $\sim 10\%$ [13]). Bechtold reported that the rate sensitivity m of re-crystallized coarse-grained W is 0.042 [45]. This value of m is about one order of magnitude larger than most fcc CG metals [46]. The high SRS of single crystal or CG bcc metals has been attributed to the unique non-coplanar core structure of screw dislocations in such lattice structures. This non-coplanar core structure implies a high Peierls–Nabarro barrier which is to be overcome by thermal activation. As a consequence, the mobility of screws is much smaller than that of edges at low homologous temperatures ($T < \sim 0.3 T_m$, T_m being the melting point in Kelvin) and the moving of screws becomes the rate-controlling mechanism in bcc metals [47,48]. Due to the non-planar core structure, screws in bcc metals move by the kink pair mechanism [47] and the thermally assisted nucleation of kink pairs is the rate-limiting step [47,49]. As outlined in [18,50], the operational activation volume of this process, v^* , is related to m by $m = \frac{2kT}{v^*}$. In UFG materials at high strain rates, v^* is on the order of a few b^3 and is almost independent of τ , grain size and dislocation density [46,50–52]. Thus m can be decreased by increasing τ , (e.g., by refining the microstructure). In other words, when the grain size is refined, the contribution to the total stress will be dominated by the long-range stresses due to grain boundaries, and the local Peierls–Nabarro barrier will contribute less. Therefore, with a UFG microstructure, the overall SRS will be reduced according to this relation [46]. Fig. 8(a) displays double-log plots for W with different

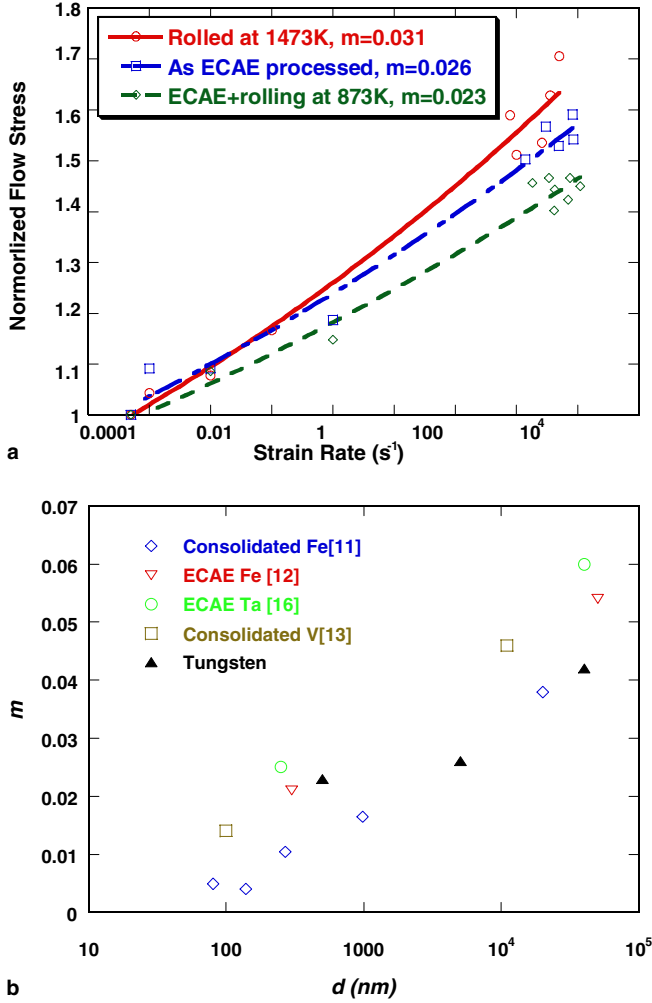


Fig. 8. (a) Strain rate sensitivity m of W after working under various conditions. The CG W of commercial purity has an m of ~ 0.04 from an early investigation [45]. (b) Strain rate sensitivity, m , is reduced monotonically with microstructure refinement into the UFG regime, in several bcc (Fe, Ta, V) metals (open symbols). The values for recrystallized and UFG-W are highlighted using solid symbols (black triangles). Here, the grain size d is a measure of the microstructural length scale, for grains and subgrains separated by both high-angle and low-angle boundaries.

microstructure (grain sizes) showing that the SRS of UFG W has been cut to half the value of the CG W. Fig. 8(b) includes our previous results on bcc Fe, Ta and V [11,13,16] showing that m can drop substantially when the grain size is refined.

Wright [3,53] provides the following quantitative description of the susceptibility to ASB

$$\frac{\chi_{SB}}{a/m} = \min \left\{ 1, \frac{1}{(n/m) + \sqrt{n/m}} \right\}, \quad (3)$$

where χ_{SB} is the susceptibility to ASB, a the non-dimensional thermal softening parameter defined by $a = (-\partial\sigma/\partial T)/\rho c$ (σ is the flow stress, T the temperature, ρ the density and c the specific heat of the material), n the strain hardening exponent and m the strain rate sensitivity. For a per-

fectly plastic material (no strain hardening) such as the SPD processed W in this work, the susceptibility reduces to

$$\chi_{SB} = \frac{a}{m} = \frac{\lambda\sigma_0}{\rho cm}, \quad (4)$$

where $\lambda = -(1/\hat{\sigma}_0)\partial\sigma/\partial T$ is the thermal softening parameter evaluated under isothermal conditions [30] ($\hat{\sigma}_0$ is a normalizing stress), and σ_0 is the yield strength. A simple calculation based on the experimental results and the physical properties of W shows that susceptibility to ASB of the UFG W is several orders of magnitude higher than that of conventional CG W.

Another way to evaluate the propensity of a metal for ASB is to estimate the critical shear strain for localization. Again, there are several models based on different assumptions about the constitutive laws of the material. The problem becomes very simple for a material without strain hardening such as is approximately the case in UFG W. Assuming an exponential dependence of the flow stress on temperature and no strain hardening, such that the constitutive law can be written as

$$\tau = \tau_0 \cdot \exp(-\alpha \cdot T) \cdot \dot{\gamma}^m, \quad (5)$$

where τ_0 is a constant, α a positive constant, T the absolute temperature and m the strain rate sensitivity. The critical shear strain for shear localization can be derived as [1]:

$$\gamma_A^c = \frac{\rho C}{\alpha \beta \tau_A^0} \left\{ \left[1 - g^{1/m} \exp(-\alpha(1-m)(T_B^0 - T_A^0)/m) \right]^{-m/(1-m)} - 1 \right\}. \quad (6)$$

In Eq. (6), τ_A^0 is the isothermal shear flow stress of the material. The factor g defines the geometric defect (taken to be unity for these compression tests) and m is the strain rate sensitivity. $(T_B^0 - T_A^0)$ describes the temperature difference between the center of the ASB and the matrix (taken to be ~ 1000 K). The experimental results by Argon and Maloof [30] on W at different temperatures can indeed be described very well by Eq. (5) with α being 0.003957. Using the above parameters for UFG W the critical shear strain is calculated to be about 0.1. Therefore, the normal critical strain for ASB will be smaller than 0.1. The high-speed photographs of Fig. 7 do show that shear bands have already occurred at a strain level of 0.1. Bearing in mind the limited spatial resolution of the high-speed camera, it is then reasonable to believe that ASB might have initiated before this strain level.

Careful examination of the quasi-static true stress–true strain curves of the UFG W (Fig. 3) indicates that the plastic part is not absolutely flat: slight strain hardening is still present. Fitting the plastic part with a power law gives a strain-hardening exponent of ~ 0.023 (more than one order of magnitude smaller than that of CG W). Assuming that the constitutive behavior of UFG W can be described by the Litonski relation as [4]

$$\tau = A\gamma^n(1 + B\dot{\gamma})^m(1 - cT), \quad (7)$$

where τ is the shear stress, γ the plastic shear strain, n the strain hardening exponent (~ 0.023 for UFG W of this

work), $\dot{\gamma}$ the plastic shear strain rate and m the SRS (usually the term $B\dot{\gamma}$ is much larger than unity, and (7) can be reduced to the power-law strain rate hardening), T the temperature, and A , B , c are materials constants. Based on Eq. (7) and stability analyses, Burns and Trucano [54] derived the following critical shear strain for a strain-hardenable metal

$$\gamma_c = \left\{ \frac{n\rho C}{Ac} \frac{1}{(1+B\dot{\gamma})^m} \right\}^{\frac{1}{n+1}}. \quad (8)$$

Experimental results [55] on W ribbons (heavily deformed at low temperature) that have room temperature flow stress close to the UFG W of this work show that their flow stresses vary as a function of temperature in the manner described by (7) with c being $\sim 0.7 \times 10^{-3}/\text{K}$. The values of other parameters to be used in Eq. (8) are: $A = \sim 1430$ MPa, $\rho = 19.25$ g/cm³ (density of W), $C = 0.134$ J/g K (specific heat of W), $B = 10^4$ s [54]. An estimate of the critical shear strain from Eq. (8) is ~ 0.046 , which corresponds to a normal strain of 0.026. We can see that even though work hardening is considered, because of its small contribution to stabilizing the plastic deformation (n is very small compared to a conventional CG-W), the estimated critical shear strain is not far from the perfect plastic assumption.

We envisage that due to the concurrent effects of much elevated flow strength and ductility, and the diminished role of the stabilizing mechanisms of strain hardening and strain rate hardening, the UFG bcc microstructure will have low resistance to softening (thermal or geometric) mechanisms. As a consequence, plastic flow will be more likely to localize. In this work, plastic flow in the form of ASB, and the subsequent cracking are indeed observed upon uniaxial high-rate compressive loading of the high-strength, ductile UFG-W (Figs. 5–7). Note (see [18]) that the SPD and grain refinement have improved the ductility at the same time as obtaining higher strength.

In the past, flow localization has often been induced by intentionally generating localized shear stresses in the sample through special design of sample geometry. For example, adiabatic shear banding has been observed in CG W samples with hat-shaped or truncated cone geometry loaded under dynamic compression [29,56,57]. In contrast, we have reported the first observation of adiabatic shear localization in commercial purity UFG W using conventional Kolsky bar compression tests [18]. Similar flow localization has been now observed in many ultrafine-structured bcc metals, for example in Fe and Ta [11,12,14,16].

5. Summary and concluding remarks

We have refined the microstructure of a coarse-grained W of commercial purity via severe plastic deformation to achieve an ultrafine microstructure. This W not only exhibits considerably elevated flow stress, it also shows significantly enhanced ductility. Mechanical testing under quasi-static and dynamic loading shows that W with such

microstructure has much reduced strain-hardening capacity (the plastic part of the true strain–true stress curve is almost flat under quasi-static loading). In addition, its strain rate sensitivity has been decreased to half that of its coarse-grained counterparts. The diminished strain hardening can be understood on the basis of the intrinsic size effect in metals on their work hardening mechanism. The reduction in strain rate sensitivity by refining the microstructure of W can be understood by invoking the dislocation mediated plastic deformation mechanism of bcc metals at relatively low homologous temperatures, i.e., kink pair nucleation and its subsequent propagation. The much enhanced ductility in the SPD processed UFG W can be attributed to the plastic-deformation-induced non-equilibrium and large angle grain boundaries which dilute away the interstitial impurities by their diffusion to and redistribution along such grain boundaries. The resulting high strength, reinstated ductility, as well as reduced strain hardening and strain rate hardening, lead to favorable conditions for the initiation of adiabatic shear localization, and the subsequent cracking observed for the first time in W under uniaxial dynamic compression [18]. The UFG-W with such a deformation mode may offer a high-density material uniquely suited for certain critical applications.

Acknowledgments

The authors thank Mr. Haitao Zhang and Dr. Yulong Li for experimental assistance. They are also grateful to Dr. T.W. Wright (Army Research Laboratory) for very helpful discussions. This work was performed at JHU-CAMCS, sponsored by ARL under the ARMAC-RTP Cooperative Agreement #DAAD19-01-2-0003.

References

- [1] Molinari A, Clifton RJ. *J Appl Mech. Trans ASME* 1987;54:806.
- [2] Bai Y. *J Mech Phys Solids* 1982;30:195.
- [3] Wright TW, Bartra RC. *Int J Plast* 1985;1:205.
- [4] Wright TW. *The physics and mathematics of adiabatic shear bands*. Cambridge: Cambridge University Press; 2002.
- [5] Bai Y, Dodd B. *Adiabatic shear localization*. New York, NY: Pergamon Press; 1992.
- [6] Magness LS, Kapoor D, Dowding R. *Mater Manuf Proc* 1995;10:531.
- [7] Bleise A, Danesi PR, Burkart W. *J Environ Radioactiv* 2003;64:93.
- [8] Cai WD, Li Y, Dowding R, Mohamed FA, Lavernia EJ. *Rev Particulate Mater* 1995;3:71.
- [9] Lassner E, Schubert W-D. *Tungsten-properties, chemistry, technology of the element, alloys and chemical compounds*. New York (NY): Kluwer Academic/Plenum Publishers; 1998.
- [10] Gumbsch P, Riedle J, Hartmaier A, Fischmeister HF. *Science* 1998;282:1293.
- [11] Jia D, Ramesh KT, Ma E. *Acta Mater* 2003;51:3495.
- [12] Wei Q, Kecskes L, Jiao T, Hartwig KT, Ma E, Ramesh KT. *Acta Mater* 2004;52:1859.
- [13] Wei Q, Jiao J, Ramesh KT, Ma E. *Scripta Mater* 2004;50:359.
- [14] Marlow TR, Koch CC. *Acta Mater* 1998;46:6459.
- [15] Carsley JE, Fisher A, Milligan WW, Aifantis E. *Metall Mater Trans A* 1998;29:2261.

- [16] Wei Q, Jiao T, Mathaudhu SN, Ma E, Hartwig KT, Ramesh KT. *Mater Sci Eng A* 2003;358:266.
- [17] Wei Q, Jia D, Ma E, Ramesh KT. *Appl Phys Lett* 2002;81:1240.
- [18] Wei Q, Ramesh KT, Ma E, Kesckes LJ, Dowding RJ, Kazykhanov VU, et al. *Appl Phys Lett* 2005;86:101907.
- [19] Lowe TC, Valiev RZ, editors. *Investigations and applications of severe plastic deformation*. Dordrecht: Kluwer Academic Publishers; 2000.
- [20] Zhu YT, Langdon TG, Mishra RS, Semiatin SL, Saran MJ, Lowe TC, editors. *Ultrafine grained materials II*, TMS annual meeting and exhibition. Warrendale, PA: TMS; 2002.
- [21] Valiev RZ, Islamgaliev RK, Alexandrov IV. *Prog Mater Sci* 2000;45:103.
- [22] Islamgaliev RK, Pyshmintsev IY, Khotinov VA, Korznikov AV, Valiev RZ. *Phys Met Metall* 1998;86:408.
- [23] Valiev RZ, Korznikov AV, Mulyukov RR. *Mater Sci Eng A* 1993;168:141.
- [24] Segal VM. *Mater Sci Eng A* 1995;197:157.
- [25] Allen BC, Maykuth DI, Jaffee RI. *J Inst Metals* 1962;90:120.
- [26] Farrell K, Schaffhauser AC, Stiegler JO. *J Less Common Metals* 1967;13:141.
- [27] Follansbee PS. The Hopkinson bar. In: Davis JR, Refnes SK, editors. *Metals handbook*, 9th ed., vol. 8. Metals Park (OH): ASM; 1985. p. 198–203.
- [28] Lennon AM, Ramesh KT. *Mater Sci Eng A* 2000;276:9.
- [29] Dummer T, Lasalvia JC, Ravichandran G, Meyers MA. *Acta Mater* 1998;46:6267.
- [30] Argon AS, Maloof SR. *Acta Metall* 1966;14:1449.
- [31] Bechtold JH, Shewmon PG. *Trans ASM* 1954;46:397.
- [32] Nes E. *Prog Mater Sci* 1998;41:129.
- [33] Doherty RD, Hughes DA, Humphreys FJ, Jonas JJ, Jensen DJ, Kassner ME, et al. *Mater Sci Eng A* 1997;238:219.
- [34] Hughes DA, Hansen N. *Acta Mater* 1997;45:3871.
- [35] Valiev RZ, Alexandrov IV, Thu YT, Lowe TC. *J Mater Res* 2002;17:5.
- [36] Valiev RZ. *Nat Mater* 2004;3:511.
- [37] Ivannisenko Y, Valiev RZ, Fecht HJ. *Mater Sci Eng A* 2005;390:159.
- [38] Zhilyaev AP, Kim BK, Nurislamova GV, Baro MD, Szpunar JA, Longdon TG. *Scripta Mater* 2002;46:575.
- [39] Hart EW. *Acta Metall* 1967;15:351.
- [40] Semiatin SL, Jonas JJ. *Formability and workability of metals*. Metals Park (OH): ASM; 1984.
- [41] Cherukuri HP, Shawki TG. *Int J Plast* 1995;11:15.
- [42] Thompson AW. *Acta Metall* 1977;25:83.
- [43] Basinski SJ, Basinski ZS. In: Nabarro FRN, editor. *Dislocations in solids*, vol. 4. Amsterdam: North-Holland; 1979. p. 261.
- [44] Sevillano JG, Arizcorreta IO, Kubin LP. *Mater Sci Eng A* 2001;309:393.
- [45] Bechtold JH. *Trans AIME* 1956;206:142.
- [46] Wei Q, Cheng S, Ramesh KT, Ma E. *Mater Sci Eng A* 2004;381:71.
- [47] Kubin LP, Devincere B, Tang M. *J Comput-Aided Mater Design* 1998;5:31.
- [48] Duesbery MS, Vitek V. *Acta Mater* 1998;46:1481.
- [49] Marian J, Cai W, Bulatov VV. *Nat Mater* 2004;3:158.
- [50] Kocks UF, Argon AS, Ashby MF. *Prog Mater Sci* 1975;19:1.
- [51] Caillard D, Martin JL. *Thermally activated mechanisms in crystal plasticity*. Oxford: Pergamon; 2003.
- [52] Rodriguez P. *Metall Mater Trans A* 2004;35:2697.
- [53] Wright TW. *Int J Plast* 1992;8:583.
- [54] Burns TJ, Trucano TG. *Mech Mater* 1982;1:313.
- [55] Boser O. *J Less-Common Met* 1971;23:427.
- [56] Li JR, Yu JL, Wei ZG. *Int J Impact Eng* 2003;28:303.
- [57] Wei ZG, Yu JL, Li JR, Li YC, Hu SS. *Int J Impact Eng* 2001; 26:843.